PCCP

Accepted Manuscript

ROYAL SOCIETY OF CHEMISTRY

www.rsc.org/pccp

Non-covalent interactions in ionic liquid ion pairs and ion pair dimers: A quantum chemical calculation analysis

Bogdan A. Marekha[1*], Oleg N. Kalugin[2], and Abdenacer Idrissi[1*]

[1]University of Lille – Science and Technology, LASIR (UMR CNRS A8516), Bat. C5, 59655, Villeneuve d'Ascq Cedex, France

[2]V.N. Karazin Kharkiv National University, Department of Inorganic Chemistry, Svoboda sq., 4, Kharkiv, 61022, Ukraine

*Corresponding authors:

bogdan.marekha@univ-lille1.fr (BAM), nacer.idrissi@univ-lille1.fr (AI).

Abstract

Ionic liquids (ILs) being composed of bulky multiatomic ions reveal a plethora of non-covalent interactions which determine their microscopic structure. In order to establish the main peculiarities of these interactions in IL-environment, we have performed quantum chemical calculations for a set of representative model molecular clusters. These calculations were coupled with advanced methods of analysis of the electron density distribution, namely, the quantum theory of atoms in molecules (QTAIM) and the non-covalent interactions (NCI; *JACS* 132 **2010** 6499) approaches. The former allows for profound quantitative characterization of non-covalent interactions between atoms while the latter gives an overview of spatial extent, delocalization, and relative strength of such interactions. The studied systems consist of 1-butyl-3-methylimidazolium ($Bmim^+$) cation and different perfluorinated anions: tetrafluoroborate (BF_4^-), hexfluorophophate (PF_6^-), trifluoromethanesulfonate (TfO^-), and bis(trifluoromethanesulfonyl)imide ($TFSI^-$). IL ion pairs and ion pair dimers were considered as model structures for the neat ILs and large aggregates. Weak electrostatic hydrogen bonding was found between the anions and the imidazolium ring hydrogen atoms of cations. Weaker but still appreciable hydrogen bonding was also noted for hydrogen atoms of the adjacent to the imidazolium ring alkyl groups of $Bmim^+$. The relative strength of the hydrogen bonding is higher in BmimTfO and $BmimBF_4$ ILs than in $BmimPF_6$ and BmimTFSI, whereas BmimTfO and BmimTFSI reveal higher sensitivity of hydrogen bonding at the different hydrogen atoms of the imidazolium ring.

Introduction

Ionic liquids (ILs) constitute a large class of substances that draw a considerable scientific interest due to their number of advantageous properties.[1] The structure of imidazolium-based ILs is mainly determined by the strong interionic Coulombic interactions which are relatively efficiently screened moving away from the central ion (*i.e.,* they are rather local).[2, 3] A significant contribution is also supposed to arise from a three-dimensional network of hydrogen bonds between the counterions[4, 5] as well as from dispersion interactions.[6, 7] The overall balance of these forces gives rise to self-association of ILs which is manifested at the microscopic level in the redistribution of electron density at specific interaction sites. These weak non-covalent interactions can contribute up to 20 percent of the overall interaction energy in ILs.[8] Recently, some efforts have been undertaken to dissect the hydrogen bonding and dispersion contributions in protic ILs from far-IR experiment and theoretical calculations.[8, 9] Apart from the binding energy perspective, a comprehensive understanding of the complete pattern of non-covalent interactions between the constituting ions and the related electron density distribution is a key prerequisite for a consistent IL characterization.

Quantum chemical electronic structure calculations have been routinely used to study various properties of the IL-based systems, to help with the analysis of experimental results and to design new potentially better performing ILs.[7, 10] One should always be cautious when trying to connect the results obtained from calculations on model systems of the size of tens of atoms, often performed in the gas phase, to subtle properties of the macroscopic samples. It is only very recently that molecular dynamics (MD) simulations of the IL-based systems of relevant size and trajectory length have become feasible.[7] Nevertheless, there is still a severe lack of proper MD force field models suitable to be applied over a broad range of conditions for ILs.[11] At present, quantum chemical calculations of small model systems are affordable for the routine use in order to reveal the electronic properties of ILs in detail.

The majority of published to date quantum chemical calculations have been performed by means of density functional theory (DFT) calculations on 1-alkyl-3-methylimidazolium IL ion pairs

(RmimX) and other representative systems.[7, 10] Most of these reports are based on the results obtained with the popular B3LYP functional,[7, 10] which is known to be relatively inaccurate in systems where dispersion plays role, including ILs.[12-16] Thus, many conclusions drawn from these calculations may turn out to be an artifact of poor description of the dispersion interactions. For example, as it was shown by Matthews *et al.*,[17] B3LYP gives wrong energy ordering of the most stable ion pair structures of MmimCl when benchmarked against the second-order Møller-Plesset perturbation theory (MP2) and coupled cluster (CCSD(T)) methods.

At present, there are two mainstream approaches to overcome this issue at little increase of computational cost. One deals with the addition of an empirical pairwise correction term, which scales as inverse sixth power of interatomic separation, as for example the one introduced by Grimme,[18] known as vdW-correction or DFT-D2. Another approach benefits from implicit parameterization of novel functionals in order to better describe medium-range dispersion effects.[19] Truhlar's Minnesota family of functionals, particularly the M06-2X,[20] are the most popular in the chemistry field. Both approaches have been found to bring about a considerable improvement of accuracy when benchmarked against high-level calculations on test datasets that consist of systems with dispersion and hydrogen bonding,[14-16] and those including IL ion pairs and larger structures.[12, 13, 21, 22] In this regard, a thorough validation of the level of theory to be used in a computational study seems to be a crucial point when it comes to the relevance of the results.

Bader's quantum theory of atoms in molecules (QTAIM)[23] is one of the well-established methodologies for the analysis of electron density distribution in molecular systems. For a given system it gives its complete bonding pattern including weak non-covalent interactions between atoms. The latter feature is highly valued in detailed studies on such interactions, particularly, on hydrogen bonds,[24, 25] including those in ILs.[4, 26] The central property of interest for QTAIM is the electron density, ρ, whose topology is characterized in terms of critical points (CPs) where the electron density gradient vanishes ($\nabla\rho = 0$). Any bonding contact between two atoms, whether covalent or non-covalent, is characterized by a bond critical point (BCP) which is at the same time a

point of minimum in ρ along a bond path and a point of maximum in the plane which is orthogonal to it. The former is a line of highest electron density connecting the two interacting atoms. Various descriptors at the BCP, such as the electron density, ρ^{BCP}, electron density Laplacian, $\Delta\rho^{BCP}$, and total electron energy density, H^{BCP}, can be used to asses the interaction strength and to distinguish between different types of weak non-covalent interactions.[24, 27] Different sets of hydrogen bonding criteria and types have been proposed in this regard[24, 28] including the very recent classification of doubly ionic hydrogen bonds between the IL counterions by Hunt and co-workers.[4]

One of the drawbacks of the QTAIM approach is that the whole analysis, which starts by locating the CPs, relies on a numerical differentiation procedure which can fail to locate the CPs, particularly the bond critical points (BCPs) corresponding to weak non-covalent interactions in the regions of low electron density.[29] In fact, there are situations described in the literature where everything points to the existence of a weak attractive non-covalent interaction, like the intramolecular hydrogen bond in ethylene glycol,[29] but QTAIM does not reveal the corresponding BCP. The problem is that the electron density gradient in the vicinity of the anticipated BCP location approaches zero, but does not reach it in terms of numerical accuracy of the QTAIM algorithm.

An approach that is capable of overcoming this problem has been recently developed by Contreras García and Johnson.[30-33] It is called 'non-covalent interactions' analysis, or NCI, and it is based on an analysis of the electron density distribution in molecular systems in the regions of low electron density and low gradient values. This approach is also often referred to as 'reduced density gradient' (RDG) analysis.[34]

$$\mathrm{RDG} = \frac{1}{2(3\pi^2)^{1/3}} \frac{|\nabla\rho|}{\rho^{4/3}} \qquad (1)$$

When RDG is plotted as a function of electron density multiplied by the sign of the electron density Hessian second eigenvalue (vide infra), $\mathrm{sign}(\lambda_2)\rho$, one can reveal and quantify different types of weak non-covalent interactions including hydrogen bonds.[29, 31, 32, 35] The NCI analysis also

provides means of visual highlighting of the regions of interest. [31, 32] This approach has been already applied to a number of dialkylimidazolium IL ion pairs[36-39] and very recently to MmimCl ion pair dimers.[26]

In the present Article, we present QTAIM and NCI analyses using a carefully selected level of theory of representative configurations of IL ion pairs and ion pair dimers based on 1-butyl-3-methylimidazolium ($Bmim^+$) cation coupled with perfluorinated anions (BF_4^-, PF_6^-, $CF_3SO_3^-$ and $(CF_3SO_2)_2N^-$). These ILs are promising candidates for electrolyte components used in different electrochemical devices both as neat liquids and in mixtures with additives.[40-42]

Computational details

Most of the quantum chemical calculations reported in this work were conducted using density functional theory (DFT) using the GAUSSIAN 09 program suite.[43] Ultrafine integration grid and the default convergence criteria were used throughout. MP2 was employed as a reference method for benchmarking purposes.

We compared the results from the DFT-D2/D3 approaches applied to the functionals B3LYP, B97, and wB97x, annotated as B3LYP-D3, B97D, and wB97xD, with ones from the M06-2X functional. Recently, Grimme even proposed parameters for the dispersion correction for the M06-2X functional, notated as M06-2X-D3[14] which was also tested here. Classical B3LYP was also included for comparison. Most of the tests were performed using Pople-type triple-zeta split-valence basis set with diffuse and polarization functions on both hydrogens and heavy elements 6-311++g(d,p). The influence of the basis set was studied for the M06-2X functional coupled with 6-31+g(d), 6-311+g(d,p), 6-311++g(d,p), and aug-cc-pvdz basis sets. Generally, at least triple-zeta basis sets are recommended for the Minnesota family of functionals.[19] However, some benchmark studies claim that M06-2X is better coupled with Dunning's type double-zeta basis set aug-cc-pVDZ.[44] The reference methods MP2 and B3LYP were additionally tested with the heavier aug-cc-pVTZ and lighter 6-31+g(d) basis sets, respectively.

Geometry optimizations were followed by harmonic frequency analysis to ensure that the obtained structures were true minima due to the absence of imaginary wavenumbers.

Binding energies were estimated in the supramolecular approximation, *i.e.*, as a difference between energy of a given complex and the sum of energies of isolated ions constituting it, taking into account zero-point vibrational energies of the species. Basis set superposition error correction was shown to be unnecessary in DFT calculations of IL ion pairs and larger clusters[17] performed with triple-zeta valence split basis set and thus it was not taken into account in the present study.

All the QTAIM and NCI calculations were performed with the MultiWFN software[34] utilizing either its default parameters or a uniform spatial grid with a step of 0.1 a.u., respectively. In order to focus on the weak non-covalent interactions, only the regions of $\rho < 0.05$ a.u. were analyzed. All the NCI isosurfaces were plotted with VMD.[45]

A detailed description of the level of theory validation procedure is presented in the ESI. Among the tested combinations 'basis set/functional' the M06-2X/6-311++g(d,p) is the best compromise judging from the structural, energetic, electronic, and bonding properties of a sample $MmimBF_4$ ion pair.

Results and Discussion

IL ion pairs

We studied several types of model systems, *e.g.*, IL ion pairs and ion pair dimers to reveal the non-covalent interactions that could be characteristic for the neat ILs and large aggregates. Given the limited size of these model systems, the results obtained in this approach should be treated rather as a hint than solid evidence.

Main structural features of the ion pairs

Ion pairs are often taken as the smallest unit to represent the main features of the neat ILs.[10, 46] They may be also interesting by themselves as representative species in dilute solutions of ILs in molecular solvents.[47] Ion pair structures for the studied set of imidazolium ILs obtained from gas-phase calculations are shown in Fig. 1. Most of the literature studies on quantum-chemical

calculations of the imidazolium IL ion pairs containing BF_4^- and PF_6^- anions suggest that the configuration where the anion sits on top of the C^2-H^2 fragment is the most stable one.[13, 48-60] When referencing to 'above' or 'on-top' of the imidazolium ring plane, it means at the same side as the alkyl chain with respect to the ring. This configuration was found in our optimizations even when other initial structures revealed by some previous investigations[48, 50, 51, 53, 58, 59, 61] were employed, *e.g.*, with anion positioned in front of the C^2-H^2 fragment or at the C^5-H^5 - $C^{\alpha}H_2$ site in the plane of the imidazolium ring. This can be explained as a result of poor performance of the B3LYP functional that was used in most of the previously cited studies. We also note rather rare usage of triple-zeta basis sets in these investigations which could lead to improper description of the potential energy surface. The on-top of C^2-H^2 arrangement of the PF_6^- anion with its three fluorine atoms pointing towards the cation was also established by Hardacre *et al.* in neutron scattering studies on $RmimPF_6$ coupled with MD simulations.[62, 63]

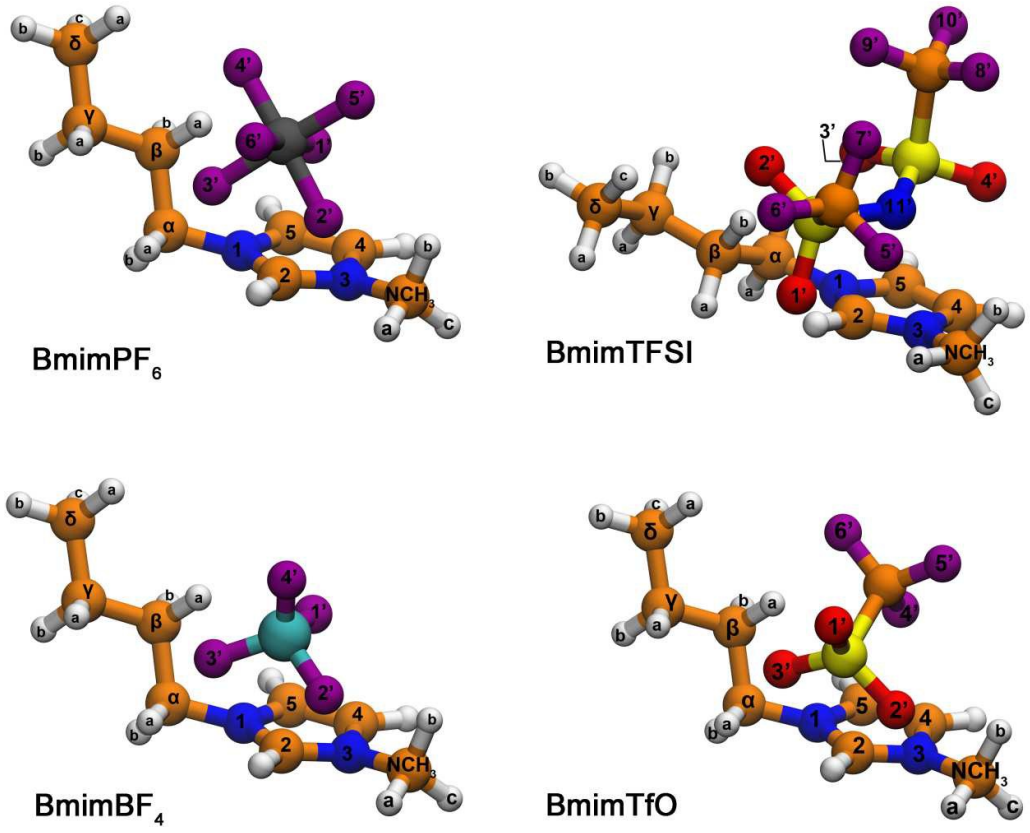

Fig. 1. Optimized in vacuum at the M06-2X/6-311++g(d,p) level of theory structures of the studied ion pairs. Color coding of the elements: white – H, orange – C, blue – N, purple – F, cyan – B, gray – P, yellow – S.

Calculations on the $TFSI^-$ containing imidazolium ILs reveal two kinds of structures. B3LYP and Hartree-Fock based studies employing rather moderate basis sets[48, 64-66] predict the anion to be in front of the C^2-H^2 fragment in the plane of the imidazolium ring. In these structures the anion was found in the trans-conformation with respect to its C-S-N-S-C fragment and strong directional hydrogen bonds were observed between the C^2-H^2 hydrogen and anion's nitrogen and/or oxygen atoms.[66] On the other hand, more recent studies on EmimTFSI ion pair, employing MP2/aug-cc-pVTZ[67] and M06/6-311++g(d,p)[68] levels of theory, revealed the $TFSI^-$ anion to be in the cis-configuration in all the stable low-energy minima and located on top of the C^2-H^2 fragment with one of its SO_2 moieties. This exactly corresponds to the structure found as the lowest energy minimum for the BmimTFSI ion pair in the present study. A remarkable point in this structure is that due to the bulkiness of the anion the butyl chain is pushed towards the in-plane orientation.

Similar feature was also observed for the BmimTFSI ion pair by Hunt *et al*. using B3LYP/6-311++g(d,p) level of theory.[53] Such orientation of the anion also agrees with the results of Hardacre *et al.*[62] that for the $TFSI^-$ anion the position above/below the imidazolium ring is even more favored than for PF_6^-.

Raman[69, 70] and MD[71] studies suggest a comparable population of the cis- and trans-conformations of the $TFSI^-$ anion in neat ILs. This contradiction can be resolved if one assumes that the trans-conformations, which are thermodynamically more stable, are more frequently found for 'free', or less bound configurations of the anion, while in tightly bound structures, like the ion pairs, the cis-conformation is stabilized by multiple bonding contacts with the counterions.

Theoretical studies on the ion pair structures of imidazolium ILs with TfO^- anions are far less ubiquitous.[48, 72-74] Our calculated optimal structure is in accordance with these reports. The strongly negatively charged SO_3 group of the anion is positioned on top of the C^2-H^2 fragment with two oxygen atoms being in the vicinity of C^2-H^2 and of the NCH_3 and $C^{\alpha}H_2$ hydrogen atoms. Trifluoromethyl group CF_3 of the anion is located exactly above the imidazolium ring center and the fluorine atoms are in close contact with the hydrogen atoms of the butyl group.

The common property of all the revealed optimal ion pair structures is presented in Fig. 2. One can easily see that the central atom of the negatively charged group of every anion (B for BF_4^-, P for PF_6^-, and S for TfO^- and $TFSI^-$) is positioned roughly on top of the C^2-H^2 fragment (the most positively charged part of the cation[75]) and its electronegative atoms are at hydrogen bonding distance away from the C^2-H^2 hydrogen atom and allegedly from the alkyl ones adjacent to the imidazolium ring.

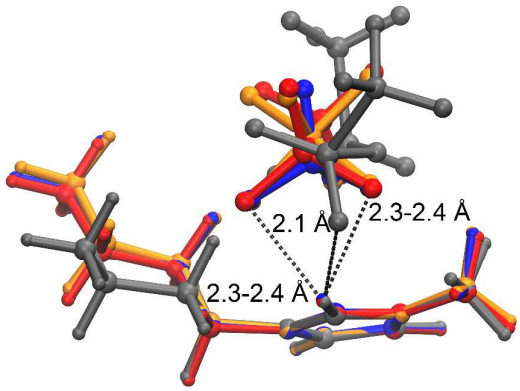

Fig. 2. Optimized in vacuum structures of the studied ion pairs, superimposed by the imidazolium ring carbon atoms. Red – BmimTfO, blue – $BmimBF_4$, orange – $BmimPF_6$, gray – BmimTFSI. Dashed lines indicate short contacts between the C^2H^2 hydrogen atoms and the nearest electronegative atoms of anion.

The general stability of the ion pairs in vacuum can be estimated with the binding energies which are −359.9, −362.8, −372.8, and −380.7 kJ mol^{-1} for $BmimPF_6$, BmimTFSI, BmimTfO, and $BmimBF_4$ respectively. The present order of ion pair binding energy values is in agreement with the literature results.[48, 73]

In order to estimate the stability of the revealed configurations with respect to the position of the anion around the imidazolium ring plane and to the rotation of the butyl chain a small supplementary survey was conducted. We performed relaxed potential energy scans along the selected dihedral angles φ and τ_2 shown in Fig. 3. The angles were varied in steps of five and fifteen degrees, respectively. A slightly smaller basis set 6-31+g(d) coupled with the M06-2X functional was used in these calculations.

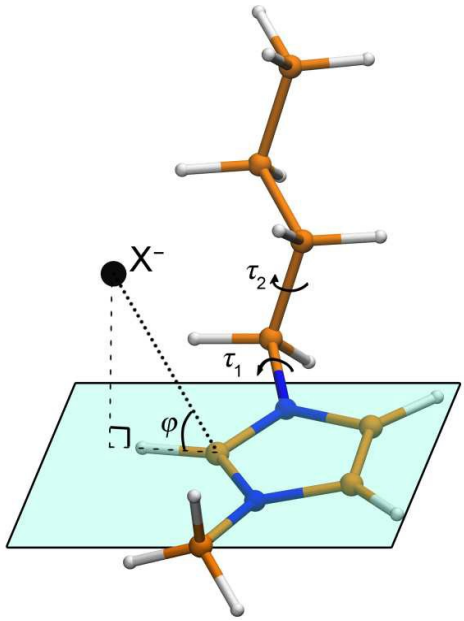

Fig. 3. Schematic representation of the main dihedral angles defining the geometry of a BmimX ion pair. The dihedrals τ_1 and τ_2 determine the orientation of the butyl chain while the φ dihedral describes the position of anion X^- relative to the imidazolium ring plane. Color coding of the elements: white – H, orange – C, blue – N, black – X.

Position of the anion relative to the imidazolium ring plane was characterized via a dihedral angle φ, which is the angle between the vector connecting the C^2 carbon with the central atom of the negatively charged group of aninon X and the imidazolium ring plane (Fig. 3). The perfect on-top-of-C^2 arrangement would correspond to the value of φ equal 90 degrees, while an in-plane arrangement is characterized by zero value of φ and the configurations where anion is below the imidazolium ring plane are found at negative φ values. In chloride-based ion pairs the in-plane configuration was found to be one of the most stable as reported in many previous computational studies.[17, 51, 53, 60, 61, 75-77] In order to figure out the effect of asymmetric alkyl substitution at the imidazolium ring as well as that of a multi/monoatomic anion on its preferential arrangement such scans along the φ dihedral were performed for $BmimBF_4$, BmimCl and MmimCl ion pairs. The results are shown in Fig. 4.

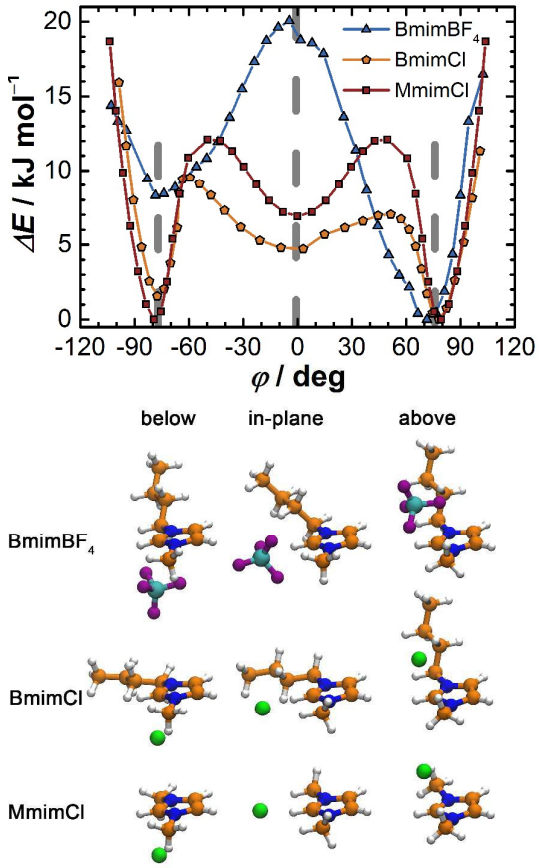

Fig. 4. Electronic energy variation during the relaxed potential energy scan along the φ dihedral for $BmimBF_4$, BmimCl, and MmimCl ion pairs obtained in vacuum at the M06-2X/6-31+g(d) level of theory (*top*). Representative structures for below, above and in-plane configurations of anions with respect to the imidazolium ring (bottom). Color coding of the elements: white – H, orange – C, blue – N, cyan – B, purple – F, green – Cl.

It is apparent that, indeed, both MmimCl and BmimCl reveal a local minimum at the in-plane configuration ($\varphi \approx 0$) in contrast to $BmimBF_4$ for which it is a maximum. The global minimum for all three ion pairs is the on-top configuration with φ equal *ca*. 80 degrees. The energy profile for MmimCl semiquantitatively agrees with the results of Zahn *et al.*[78] obtained at MP2/aug-cc-pVTZ//MP2/cc-pVTZ level of theory. We note that the asymmetry of $Bmim^+$ cation is reflected in the asymmetry of the potential energy profile, *i.e.*, the on-top of the C^2-H^2 fragment minimum structure is more stable than the one below it. This effect is more pronounced for $BmimBF_4$ (8 kJ mol^{-1}) than for BmimCl (1.5 kJ mol^{-1}), because in the latter case the chloride anion stabilizes the below-the-ring arrangement by forcing the butyl chain to be in the plane of the ring and maintaining short contacts with the alkyl hydrogen atoms of the butyl chain. From the

representative ion pair configurations shown in the bottom of Fig. 4, one can see that both for BmimCl and $BmimBF_4$ when going from the on-top configuration to the in-plane one, anion pulls the butyl chain towards the in-plane orientation. In the case of BmimCl such orientation of the butyl chain is maintained even with anion being below the imidazolium ring plane, while for the situations where BF_4^- is below the plane the butyl chain relaxes to its equilibrium out-of-plane (above) orientation.

This potential energy scan survey allowed us to claim that the on-top of C^2-H^2 arrangement of a multiatomic anion in the structure of $Bmim^+$-based IL ion pairs is rather stable and the corresponding structures obtained in our geometry optimizations can be considered as global minima. Another noteworthy point concerns the credibility of chloride based ion pairs as models for ILs with multiatomic anions. Before the computational resources became ubiquitously available to researchers, the chloride-based ILs had been considered in the first place for the sake of computational cost even though ILs with multiatomic anions present a much broader interest. Our present results suggest that one should be cautious when using the results previously obtained for chloride based ion pairs to deal with multiatomic anions as the potential energy surfaces and, hence, the representative structures can be substantially different.

The second set of potential energy scan calculations was undertaken in order to find out the influence of the butyl chain rotation on the stability of the ion pair structure. Rotation around the τ_1 dihedral was studied in detail by Hunt and Gould.[76] They showed for the front in-plane structure of BmimCl ion pair that the butyl chain strongly prefers to be oriented out of plane of the imidazolium ring regardless of its conformation and the position of anion. However, the range of values for the τ_1 dihedral was found to be rather broad.[76] Here we study the rotation along the τ_2 dihedral for the optimal configurations of the ion pairs and of the isolated $Bmim^+$ cation.

The potential energy profiles, which are shown in the top left panel of Fig. 5, are similar between the ion pairs and the isolated cation in terms of position of the extrema and the barrier heights. For the isolated cation, one of its gauche-conformations of the butyl chain ($\tau_2 \approx 300$

degrees) corresponds to the global minimum, while in all the ion pairs the trans-conformation ($\tau_2 \approx 180$ degrees) is the most stable. This result is in accordance with the literature.[76, 79-81] Variations of τ_2 do not alter significantly the τ_1 value for the isolated cation and all the ion pairs except for the BmimTFSI (bottom left panel of Fig. 5). As it was mentioned before, due to the bulkiness of the $TFSI^-$ anion, the butyl chain is close to the in-plane orientation, however, rotation about the τ_2 dihedral forces it to deviate significantly from the equilibrium orientation.

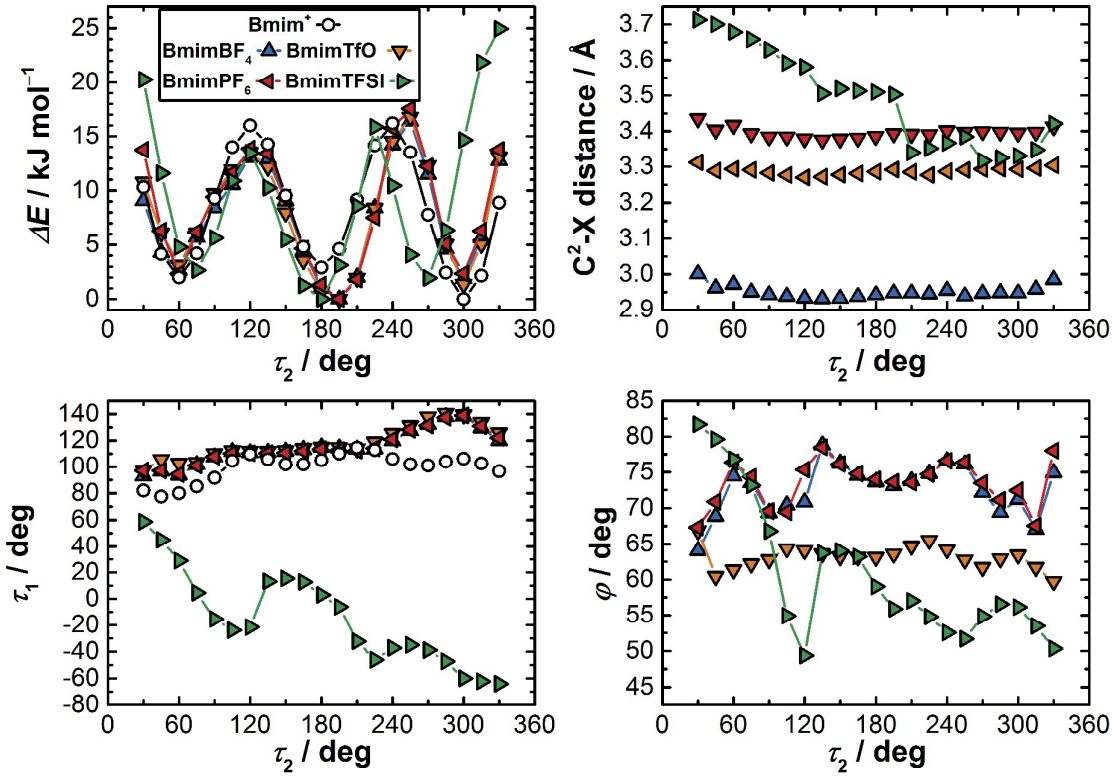

Fig. 5. The results of relaxed potential energy scan along the τ_2 dihedral for $Bmim^+$ cation and the studied ion pairs obtained in vacuum at the M06-2X/6-31+g(d) level of theory. Top left panel shows the energy variation relative to the lowest energy structure. The variations of the distance C^2-X (X=B for BF_4^-, P for PF_6^-, S for TfO^-, and the nearest S for $TFSI^-$) as a function of the scanned variable are given in the top right panel. Bottom right panel shows how the τ_1 dihedral changes as the τ_2 is varied. Bottom right panel present the φ dihedral as a function the scanned variable.

Similar observations can be made for the interionic separation characterized as the distance between the cation's C^2 carbon atom and the central atom of the negatively charged group of anion, X (top right panel Fig. 5). The variations in the scanned variable do not induce changes in the interionic separation higher than 0.05 Å for $BmimBF_4$, $BmimPF_6$, and BmimTfO ion pairs. The distance C^2-S in the BmimTFSI ion pair can vary by as much as 0.4 Å.

Relative position of anion with respect to the imidazolium ring plane, in terms of the φ dihedral values (bottom right panel of Fig. 5), follows the same trends as the interionic separation. In $BmimBF_4$, $BmimPF_6$ and BmimTfO anions remain on top of the C^2-H^2 fragment during the rotation of the butyl chain around the C^α-C^β bond and the corresponding dihedral variations do not exceed 10 degrees. In contrast, the $TFSI^-$ anion shows rather broad distribution of the φ dihedral values.Numerous Raman investigations[82-86] claim the coexistence of different conformers stemming from the rotation around the τ_2 dihedral in the neat $Bmim^+$ based ILs. Our results show that the corresponding rotation of the butyl chain has almost the same energy profile for the studied ILs and, hence, does not depend markedly on the anion. Moreover, the principal position of anion on top of the C^2-H^2 fragment of anion is hardly influenced by the rotation of the butyl chain around the C^α-C^β bond for all the IL ion pairs except BmimTFSI. The latter exhibits particular behavior which reflects that its structure is rather labile and the anion is evidently mobile and it can change its position around the equilibrium one to a considerable extent already as a consequence of the butyl chain rotation.

Altogether, these findings justify our selection of the on-top configurations of the ion pairs with cations in trans-conformations as the representative structures for subsequent analysis of weak non-covalent interionic interactions and for investigation of larger aggregates like ion pair dimers. Some literature reports also suggest that the butyl chain conformation does not influence the interionic interactions in analogous ion pairs, since they are mainly localized at the imidazolium ring.[50, 76] The results on the BmimTFSI ion pair should be interpreted cautiously though.

Weak non-covalent interactions in the IL ion pairs

Fig. 6 shows the NCI surfaces and the CPs, revealed by the QTAIM analysis, for the studied ion pairs. Similarly to the case of $MmimBF_4$ ion pair (see ESI), there are broad surfaces of weak non-covalent contacts in the interionic space.

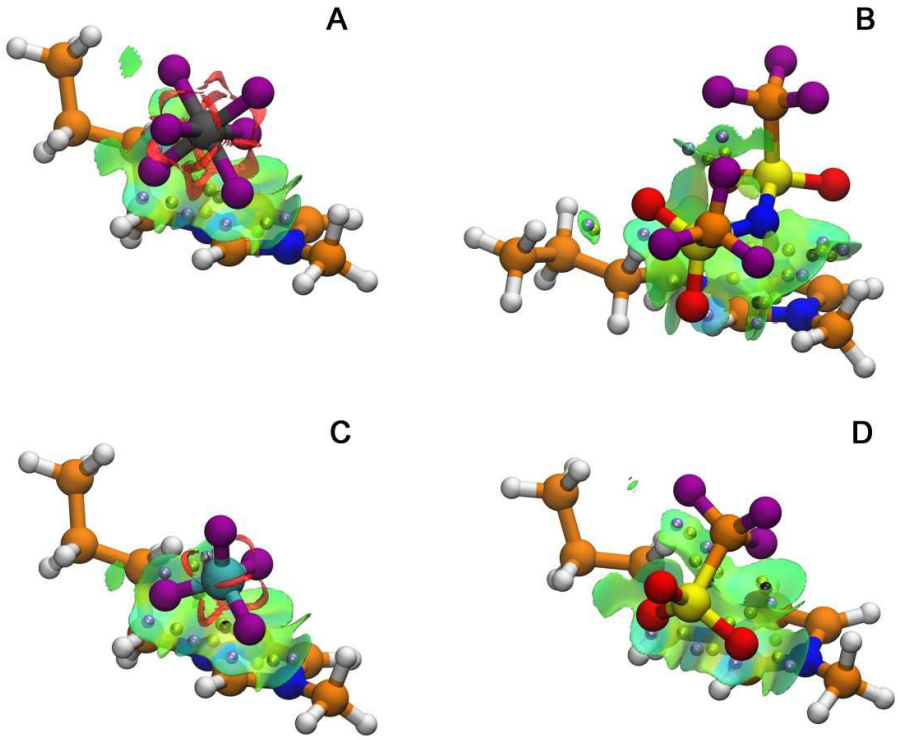

Fig. 6. NCI isosurfaces for the $BmimPF_6$ (A), BmimTFSI (B), $BmimBF_4$ (C), and BmimTfO (D) ion pair structures obtained at the M06-2X/6-311++g(d,p) level of theory in vacuum. The RDG isovalue is 0.6. The sign(λ_2)ρ value is colormapped onto the isosurfaces in the region from −0.03 a.u. to +0.03 a.u. in the blue-green-red palette. QTAIM revealed CPs are depicted as light blue (BCPs), green (RCPs), and black (CCPs) spheres. Color coding of the elements: white – H, orange – C, blue – N, purple – F, cyan – B, gray – P, yellow – S.

In all the ion pairs, the most blueish regions and the corresponding BCPs are observed in the zones of multiple contacts between the most electronegative atoms of anions (F in BF_4^- and PF_6^-, and O in TfO^- and $TFSI^-$) and the C^2-H^2 fragment. Less intense interactions, which appear as cyan or blue-green regions of the NCI surfaces, are observed for the contacts between anions and the alkyl hydrogen atoms of the NCH_3 and $C^{\alpha}H^2$ groups. The importance of the latter type of hydrogen bond like contacts for additional stabilization of cation-anion complexes has been previously emphasized in MD simulations of BmimCl and EmimCl,[87] crystal structure analysis of a series of $RmimPF_6$ ILs,[88] and in a very recent NMR study on isotopic substitution effects.[89]

The general extent of the NCI surfaces corresponding to the same RDG isovalue for all the ion pairs presented in Fig. 6, *i.e.*, the area of non-covalent contacts, is higher for larger anions. For example, for the region of interaction between the anion and the $C^{4\text{-}5}$ site, in the case of small BF_4^-

anion and the slightly larger PF_6^-, there is only a small part of green NCI isosurface typical for van der Waals like weak interaction, while for the larger TfO^- the isosurface extends closer to the $C^{4\text{-}5}$ side of the imidazolium ring and even several CPs are found there. For the largest anion studied here, $TFSI^-$, the NCI isosurface covers the entire imidazolium ring and the corresponding BCPs with the $C^{4\text{-}5}$ fragment are in the light blue region of the surface, indicating a weak attractive bonding interaction. We also note that in the NCI isosurfaces of weak dispersive contacts between the butyl chain and anions, there are no CPs found.

Quantitative results of the QTAIM analysis of the weak non-covalent interactions between the counterions in the studied IL ion pairs are collected in Fig. 7. The main BCP characteristics, such as the electron density (ρ^{BCP}), the electron density Laplacian ($\Delta\rho^{BCP}$), and the total electronic energy density (H^{BCP}) values are plotted as a function of interatomic distance in Fig. 7.

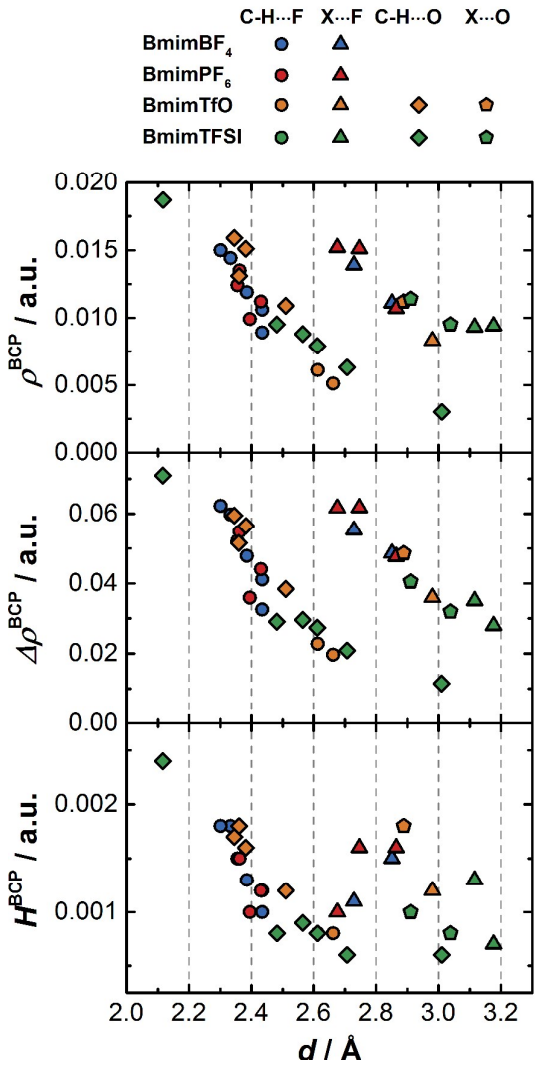

Fig. 7. The BCP electron density (top panel), electron density Laplacian (middle panel), and total electron energy density (bottom panel) values for the weak non-covalent interactions as a function of distance between the interacting atoms, as revealed in the structures of the studied ion pairs by means of QTAIM analysis. X indicates any non-hydrogen atom of the cation, *i.e.*, carbon or nitrogen.

Two distinct types of BCPs are observed. The first is between the electronegative atoms of the anions and the hydrogen atoms of the cation. The corresponding values of the electron density descriptors are in accordance with previous reports on similar systems.[4, 56, 90-92] The second BCP type corresponds to the curved bond paths. It connects the anion not with cation's hydrogen atoms, but with the adjacent carbon atoms (see $F^{2\text{-}3}\cdots C^{2}$ contacts in Fig. ESI3). Direct bonding non-covalent contacts between non-hydrogen atoms, *e.g.*, $F^{1}\cdots C^{2}$ in Fig. ESI3, fall in this BCP type as well.

The BCPs of the second type are logically found at slightly higher interatomic distances (Fig. 7). Almost linear correlations between the selected BCP descriptors and the corresponding distances are observed for both types of contacts (somewhat worse for H^{BCP}).

Also, both types of contacts have very close range of the electron density values at the BCPs, though somewhat higher for the contacts with hydrogen atoms. Given the values of ρ^{BCP}, as well as the signs of $\Delta\rho^{BCP}$ and H^{BCP}, these contacts should be classified as weak bonding contacts of electrostatic nature. The contacts with the hydrogen atoms can thus be classified as weak hydrogen bonds.[4, 24, 28] For the sake of clarity, hereafter, we will only use the ρ^{BCP} values to characterize the strength of these interactions within the QTAIM approach.

As it was noted before, BmimTFSI reveals the broadest interatomic NCI surface. This is naturally reflected in the higher number of BCPs revealed. We also note that it exhibits the shortest (≈ 2.1 Å) and strongest ($\rho^{BCP} \approx 0.019$ a.u.) hydrogen bond within the studied set of IL ion pairs. It is established between the C^2-H^2 hydrogen atom of the cation and the $O^{1'}$ oxygen atom of the anion and can be noted as the most blueish zone in the corresponding NCI isosurface. Nevertheless, we consider the occurrence of this BCP rather as an artifact than a strong persistent interaction, if one takes into account the mentioned above lability of the structure of this ion pair.

Ion pair dimers

In several theoretical studies[17, 21, 26, 55, 59, 73, 74, 77, 93] it has been claimed that the smallest unit capable to represent the main structural features of neat imidazolium-based ILs is not the ion pair but rather its dimer. Taking these considerations into account we also undertook a study on the ion pair dimers in order to model IL network structures and to understand the possible changes in the electronic structure when the size of ion aggregates is decreased upon dilution in a solvent.[47, 94] Given that the possible number of stable ion pair dimer structures is obviously large and their extensive search is rather computationally expensive and, in fact, out of scope of this study, we took advantage of the results of Matthews *et al.*[17, 74] who performed a systematic study on the ion pair dimers of MmimCl/BF_4/NO_3/CH_3SO_4/TfO at the B3LYP-D3/6-311+g(d,p) level of theory. The

most stable structures were found to be with imidazolium cations in a stacked antiparallel arrangement and with each anion interacting with the C^2-H^2 site of one cation and the C^{4-5}-H^{4-5} site of the other one. Cations can be offset from the perfect stacked antiparallel arrangement rather easily depending on anion. Danten *et al.* studied the same set of ILs, however, their attention was focused on the spectral signatures of interaction with water and the interaction between the IL constituting species were not thoroughly analyzed.[73]

We constructed the initial configurations of the ion pair dimers in accordance with the results of Matthews *et al.*[17, 74] The optimized structures are shown in Fig. 8 along with the corresponding NCI surfaces. The structures of the ion pair dimers revealed in our calculations at the M06-2X/6-311++g(d,p) level of theory are in good agreement with the results of Danten *et al*.[55, 73, 93] obtained for the same set of ion pair dimers at the B3LYP/6-31+g(d) level of theory. We also note that the butyl chains of the neighboring cations point to the opposite directions. This is in consonance with the local cation-cation arrangement revealed via NOESY NMR techniques by Mele *et al.*[95]

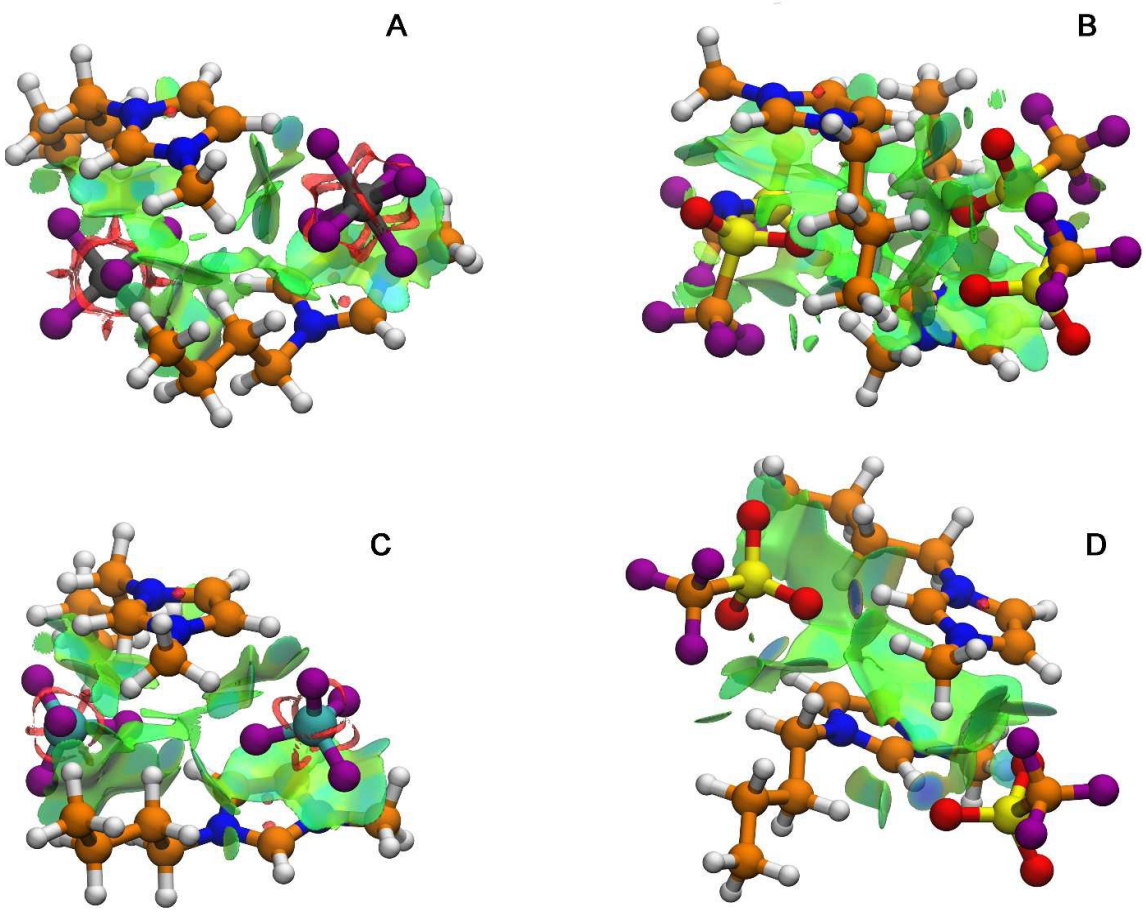

Fig. 8. NCI isosurfaces for the $BmimPF_6$ (A), BmimTFSI (B), $BmimBF_4$ (C), and BmimTfO (D) ion pair dimer structures obtained at the M06-2X/6-311++g(d,p) level of theory in vacuum. The RDG isovalue is 0.6. The sign(λ_2)ρ value is colormapped onto the isosurfaces in the region from −0.03 a.u. to +0.03 a.u. in the blue-green-red palette. Color coding of the elements: white – H, orange – C, blue – N, purple – F, cyan – B, gray – P, yellow – S.

Upon inspection of the NCI surfaces depicted in Fig. 8 several features become apparent. In addition to the obvious increase of area of weak non-covalent interactions between the ions, there are some areas of contact between cations. Particularly, in the case of BmimTfO, cations are the least displaced from the stacked arrangement and the corresponding NCI surface of weak dispersion interaction extends over the whole space between the imidazolium rings. A similar observation by Matthews *et al.* for certain MmimCl ion pair dimers has been attributed to $\pi^+\cdots\pi^+$ interactions between the cations.[26] We also note the increased number and strength of the cation-anion bonding contacts and hydrogen bonds seen as blueish regions. This is a result of expelling of the anions from the on top of C^2 arrangement, compared to ion pair structures, towards more in-plane like positions

where the hydrogen bond like directional arrangements are more favored. These contacts are also observed at the C^{4-5}-H^{4-5} sites.

The electron density values of the BCPs revealed by the QTAIM analysis of the ion pair dimer structures are plotted as a function of the distance between the interacting atoms in Fig. 9. The most important interactions with the imidazolium ring atoms are marked. The noted above increase of the number of bonding contacts is reflected in the higher number of BCPs found. This is particularly apparent for the weak contacts of low electron density ($\rho < 0.01$ a.u.) for all the investigated ILs.

As for the BCPs involving the imidazolium ring sites, we note that for $BmimBF_4$ and $BmimPF_6$ ion pair dimers the BCPs with the C^2-H^2 fragment are insignificantly influenced in terms of the corresponding distances and the electron density values, whereas the newly revealed bonding contacts with the C^5-H^5 site are of comparable or even slightly higher strength. In contrast, in the case of BmimTfO and BmimTFSI ion pair dimers a remarkable number of BCPs are revealed at significantly higher ρ^{BCP} values compared to the corresponding ion pairs. This enhancement of the strength of hydrogen bonding is particularly prominent for the C^2-H^2 hydrogen while the hydrogen bonds with the C^{4-5}-H^{4-5} sites are only slightly stronger than the hydrogen bonds in the parent ion pairs. These observations are different from those of Matthews *et al.*[26] where partially covalent strong hydrogen bonds between chloride anions and ring hydrogen atoms of $Mmim^+$ cations in ion pairs got significantly weaker upon ion pair dimer formation.

All the bonding contacts between the counterions in the ion pair dimer structures fall on the same trend lines that were established for the corresponding ion pairs (Fig. 7). The BCPs that do not obey these trends are related to the very weak contacts like H-H between the cations (squares in Fig. 9) and to the stacking interactions in the case of BmimTfO (down triangles in Fig. 9).

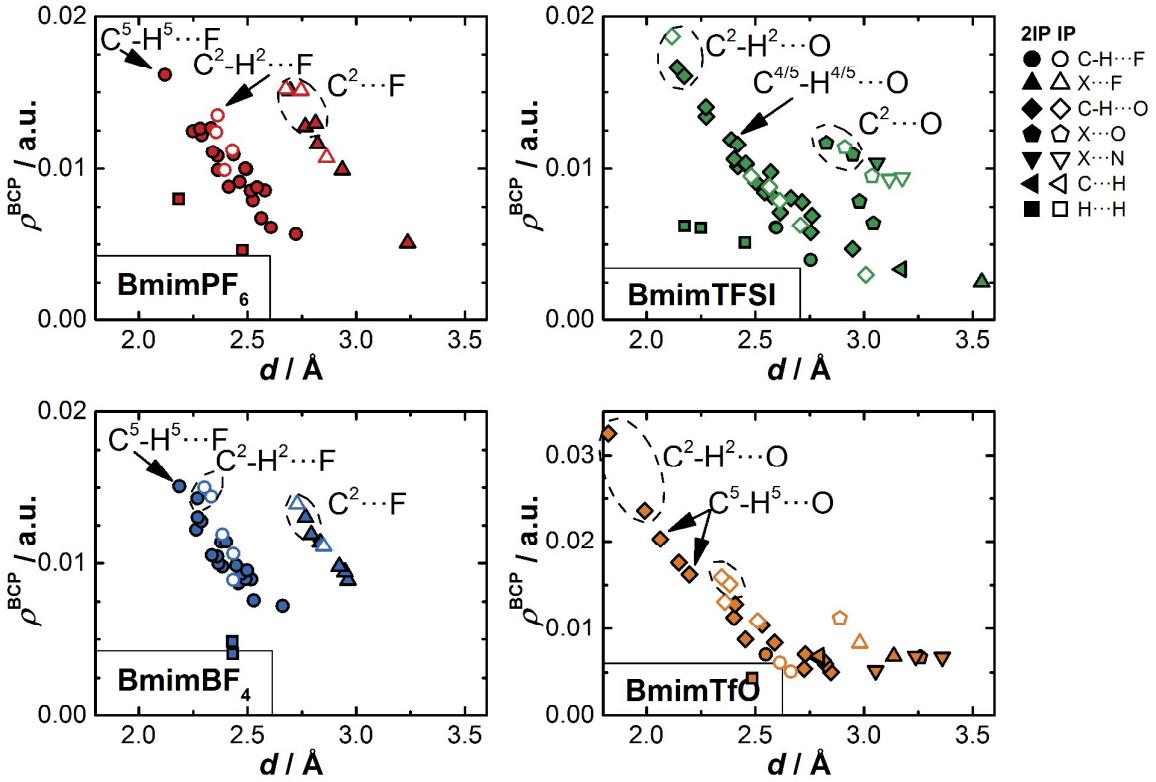

Fig. 9. The BCP electron density values for the weak non-covalent interactions as a function of distance between the interacting atoms, as revealed by means of QTAIM analysis in the structures of the studied ion pairs (open symbols) and ion pair dimers (filled symbols). X indicates any non-hydrogen atom of the cation, *i.e.*, carbon or nitrogen.

Fig. 10 presents the NCI plots of the ion pairs and the corresponding ion pair dimers. The higher number of spikes and data points in the region of weak nonbonding interactions ($\rho < 0.01$ a.u.) observed for the ion pair dimers is the reflection of the broader extent of the corresponding NCI surfaces. The strongest bonding interactions are of comparable strength between the ion pairs and ion pair dimers in the case of $BmimBF_4$ and $BmimPF_6$. A significant increase of the strength is observed for BmimTfO. For BmimTFSI, given that the spike at *ca.* −0.019 a.u. stems from the allegedly unstable hydrogen bond at the C^2-H^2 site in the ion pair structure and should be thus neglected, the enhancement of the strength of the bonding interactions is also noticed.

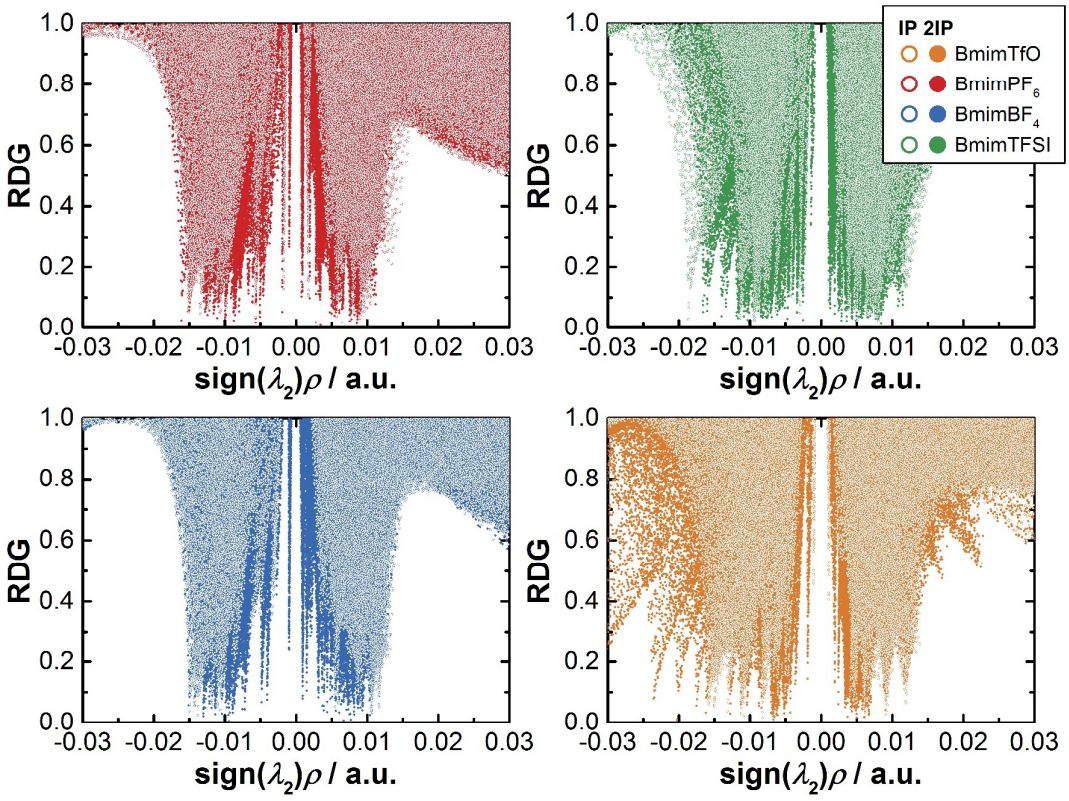

Fig. 10. The NCI plots for the structures of the studied ion pairs (open symbols) and ion pair dimers (filled symbols).

Conclusions

Quantum chemical DFT calculations of the representative structures of model clusters of ILs with multiatomic perfluorinated anions ($BmimBF_4$, $BmimPF_6$, BmimTfO, and BmimTFSI) have been used to analyze the main structural features and weak non-covalent interactions. These systems are considered as model ones which, despite limited size, can help to gather the most relevant information on the non-bonding interactions within IL-based systems. Advanced methods of analysis of the electron density distribution and of the weak non-covalent interactions have been employed to capture the details and relative strength of hydrogen bonds and other types of weak interactions in the studied systems. We still stress that larger high-level calculations are needed in order to properly capture collective effects relevant for bulk properties of ILs.

Using $MmimBF_4$ ion pair as a model object, we have shown that reliable geometrical structure and, hence, the related bonding pattern cannot be obtained with the popular B3LYP

functional as well as with such dispersion corrected functionals as B97D and wB97xD. It is only the B3LYP-D3 and implicitly parameterized M06-2X functionals that give adequate results at a reasonable computational cost. The latter one coupled with 6-311++g(d,p) basis set was used for its slightly better performance.

All the studied ILs have revealed the ion pair configuration with anion positioned on top of the C^2-H^2 fragment as the most stable one. Such arrangement of the counterions is hardly influenced by the cation's butyl chain rotation. The potential energy profile of anion's position with respect to the imidazolium ring plane is substantially different from that previously found for monoatomic anions. In the on top configuration, multiatomic anions form weak interionic electrostatic hydrogen bonds with the C^2-H^2 imidazolium ring hydrogen atom. Slightly weaker hydrogen bonds are also established with the hydrogen atoms of the adjacent alkyl groups. A number of additional stabilizing non-covalent contacts different from hydrogen bonding are observed between the counterions seen as RCPs, CCPs, and non-conventional BCPs or as broad green NCI isosurfaces indicative of dispersion interactions.

In larger aggregates, represented by ion pair dimers, hydrogen bonding at the $C^{4\text{-}5}$-$H^{4\text{-}5}$ sites is observed in addition to the interactions with the C^2-H^2 fragment. In BmimTfO and BmimTFSI, the higher strength of the hydrogen bond at the C^2-H^2 site is more apparent than in the case of $BmimBF_4$ and $BmimPF_6$. Apart from the localized hydrogen bonding interactions, there are multiple delocalized weak non-covalent interactions between the counterions and some signatures of $\pi^+\cdots\pi^+$ interactions between cations manifested in numerous BCPs, RCPs, and CCPs in the interionic space as well as in larger extent of the NCI isosurfaces.

QTAIM analysis has shown that BCP densities fall on the same linear trends as a function of distance between the interacting atoms for all the studied systems. NCI results are in excellent agreement with those from QTAIM, in particular with respect to the hydrogen bond strength in ILs which is comparable between $BmimBF_4$, $BmimPF_6$, BmimTFSI and slightly stronger for BmimTfO.

Finally, the multiple weak non-covalent interactions with a broadly distributed in space dispersion contribution seem to be a universal feature of the studied set of ILs with multiatomic perfluorinated anions. These interactions are very important in the absence of strong directional hydrogen bonds like those in ILs with small strongly basic anions, *e.g.*, NO_3^- or Cl^-. This ensemble of non-covalent forces should be given a proper attention if one wishes to rationalize the non-covalent bonding patterns in bulk ILs.

Acknowledgements

This project was supported by the Marie Curie program IRSES (International Research Staff Exchange Scheme, GAN°247500). The Centre de Ressources Informatiques (CRI) de l'Université de Lille is thankfully acknowledged for the CPU time allocation. Dr. Ari P. Seitsonen is thanked for valuable suggestions on the manuscript.

References

1. M. Smiglak, J. M. Pringle, X. Lu, L. Han, S. Zhang, H. Gao, D. R. MacFarlane and R. D. Rogers, *Chem. Commun.*, 2014, **50**, 9228-9250.
2. K. Angenendt and P. Johansson, *J. Phys. Chem. C*, 2010, **114**, 20577-20582.
3. K. Wendler, S. Zahn, F. Dommert, R. Berger, C. Holm, B. Kirchner and L. Delle Site, *J. Chem. Theory Comput.*, 2011, **7**, 3040-3044.
4. P. A. Hunt, C. R. Ashworth and R. P. Matthews, *Chem. Soc. Rev.*, 2015, **44**, 1257-1288.
5. K. Fumino, T. Peppel, M. Geppert-Rybczynska, D. H. Zaitsau, J. K. Lehmann, S. P. Verevkin, M. Kockerling and R. Ludwig, *Phys. Chem. Chem. Phys.*, 2011, **13**, 14064-14075.
6. E. I. Izgorodina, D. Golze, R. Maganti, V. Armel, M. Taige, T. J. S. Schubert and D. R. MacFarlane, *Phys. Chem. Chem. Phys.*, 2014, **16**, 7209-7221.
7. S. Zahn, M. Brehm, M. Brüssel, O. Hollóczki, M. Kohagen, S. Lehmann, F. Malberg, A. S. Pensado, M. Schöppke, H. Weber and B. Kirchner, *J. Mol. Liq.*, 2014, **192**, 71-76.
8. R. Ludwig, *Phys. Chem. Chem. Phys.*, 2015, **17**, 13790-13793.
9. K. Fumino, V. Fossog, P. Stange, D. Paschek, R. Hempelmann and R. Ludwig, *Angew. Chem., Int. Ed.*, 2015, **54**, 2792-2795.
10. B. Kirchner, in *Ionic Liquids*, ed. B. Kirchner, Springer-Verlag, Berlin/Heidelberg, 2010, vol. 290, pp. 213-262.
11. V. V. Chaban and O. V. Prezhdo, *J. Phys. Chem. Lett.*, 2013, **4**, 1423-1431.
12. C. Fong-Padrón, E. M. Cabaleiro-Lago and J. Rodríguez-Otero, *Chem. Phys. Lett.*, 2014, **593**, 181-188.
13. S. Chen, R. Vijayaraghavan, D. R. MacFarlane and E. I. Izgorodina, *J. Phys. Chem. B*, 2013, **117**, 3186-3197.
14. L. Goerigk and S. Grimme, *Phys. Chem. Chem. Phys.*, 2011, **13**, 6670-6688.
15. L. Goerigk, H. Kruse and S. Grimme, *ChemPhysChem*, 2011, **12**, 3421-3433.
16. A. Li, H. S. Muddana and M. K. Gilson, *J. Chem. Theory Comput.*, 2014, **10**, 1563-1575.
17. R. P. Matthews, T. Welton and P. A. Hunt, *Phys. Chem. Chem. Phys.*, 2014, **16**, 3238-3253.
18. S. Grimme, *Wiley Interdiscip. Rev.: Comput. Mol. Sci.*, 2011, **1**, 211-228.
19. R. Peverati and D. G. Truhlar, *Philos. Trans. R. Soc., A*, 2014, **372**, 1-81.
20. E. G. Hohenstein, S. T. Chill and C. D. Sherrill, *J. Chem. Theory Comput.*, 2008, **4**, 1996-2000.
21. E. I. Izgorodina, J. Rigby and D. R. MacFarlane, *Chem. Commun.*, 2012, **48**, 1493-1495.
22. M. A. Addicoat, S. Fukuoka, A. J. Page and S. Irle, *J. Comput. Chem.*, 2013, **34**, 2591-2600.
23. R. F. W. Bader, *Chem. Rev.*, 1991, **91**, 893-928.
24. S. J. Grabowski, *Chem. Rev.*, 2011, **111**, 2597-2625.
25. S. Grabowski, *J. Mol. Model.*, 2013, **19**, 4713-4721.
26. R. P. Matthews, T. Welton and P. A. Hunt, *Phys. Chem. Chem. Phys.*, 2015, DOI: 10.1039/C5CP00459D.
27. C. F. Matta and R. J. Boyd, eds., *The Quantum Theory of Atoms in Molecules*, Wiley, 2007.
28. U. Koch and P. L. A. Popelier, *J. Phys. Chem.*, 1995, **99**, 9747-9754.
29. J. R. Lane, J. Contreras-García, J.-P. Piquemal, B. J. Miller and H. G. Kjaergaard, *J. Chem. Theory Comput.*, 2013, **9**, 3263-3266.
30. J. Contreras-García, M. Calatayud, J.-P. Piquemal and J. M. Recio, *Comput. Theor. Chem.*, 2012, **998**, 193-201.
31. J. Contreras-García, E. R. Johnson, S. Keinan, R. Chaudret, J.-P. Piquemal, D. N. Beratan and W. Yang, *J. Chem. Theory Comput.*, 2011, **7**, 625-632.
32. E. R. Johnson, S. Keinan, P. Mori-Sánchez, J. Contreras-García, A. J. Cohen and W. Yang, *J. Am. Chem. Soc.*, 2010, **132**, 6498-6506.
33. A. Otero-de-la-Roza, E. R. Johnson and J. Contreras-Garcia, *Phys. Chem. Chem. Phys.*, 2012, **14**, 12165-12172.
34. T. Lu and F. Chen, *J. Comput. Chem.*, 2012, **33**, 580-592.

35. J. Contreras-García, W. Yang and E. R. Johnson, *J. Phys. Chem. A*, 2011, **115**, 12983-12990.
36. K. Dong and S. Zhang, *Chem. – Eur. J.*, 2012, **18**, 2748-2761.
37. L. del Olmo, C. Morera-Boado, R. López and J. García de la Vega, *J. Mol. Model.*, 2014, **20**, 1-10.
38. Y. Zheng, J. Liu, X. Yang and J. Wang, *J. Mol. Model.*, 2014, **20**, 1-11.
39. M. V. Velarde, M. Gallo, P. A. Alonso, A. D. Miranda and J. M. Dominguez, *J. Phys. Chem. B*, 2015, DOI: 10.1021/acs.jpcb.5b00229.
40. K. Matsumoto and R. Hagiwara, *J. Fluorine Chem.*, 2007, **128**, 317-331.
41. H. Xue, R. Verma and J. n. M. Shreeve, *J. Fluorine Chem.*, 2006, **127**, 159-176.
42. T. Nishida, Y. Tashiro and M. Yamamoto, *J. Fluorine Chem.*, 2003, **120**, 135-141.
43. M. J. Frisch, G. W. Trucks, H. B. Schlegel, G. E. Scuseria, M. A. Robb, J. R. Cheeseman, G. Scalmani, V. Barone, B. Mennucci, G. A. Petersson, H. Nakatsuji, M. Caricato, X. Li, H. P. Hratchian, A. F. Izmaylov, J. Bloino, G. Zheng, J. L. Sonnenberg, M. Hada, M. Ehara, K. Toyota, R. Fukuda, J. Hasegawa, M. Ishida, T. Nakajima, Y. Honda, O. Kitao, H. Nakai, T. Vreven, J. A. J. Montgomery, J. E. Peralta, F. Ogliaro, M. Bearpark, J. J. Heyd, E. Brothers, K. N. Kudin, V. N. Staroverov, T. Keith, R. Kobayashi, J. Normand, K. Raghavachari, A. Rendell, J. C. Burant, S. S. Iyengar, J. Tomasi, M. Cossi, N. Rega, J. M. Millam, M. Klene, J. E. Knox, J. B. Cross, V. Bakken, C. Adamo, J. Jaramillo, R. Gomperts, R. E. Stratmann, O. Yazyev, A. J. Austin, R. Cammi, C. Pomelli, J. W. Ochterski, R. L. Martin, K. Morokuma, V. G. Zakrzewski, G. A. Voth, P. Salvador, J. J. Dannenberg, S. Dapprich, A. D. Daniels, O. Farkas, J. B. Foresman, J. V. Ortiz, J. Cioslowski and D. J. Fox, *Gaussian 09, Revision D.01*, (2013) Gaussian, Inc., Wallingford CT.
44. J. A. Plumley and J. J. Dannenberg, *J. Comput. Chem.*, 2011, **32**, 1519-1527.
45. W. Humphrey, A. Dalke and K. Schulten, *J. Mol. Graphics*, 1996, **14**, 33-38.
46. S. Koßmann, J. Thar, B. Kirchner, P. A. Hunt and T. Welton, *J. Chem. Phys.*, 2006, **124**, 174506.
47. H. K. Stassen, R. Ludwig, A. Wulf and J. Dupont, *Chem. – Eur. J.*, 2015, DOI: 10.1002/chem.201500239.
48. S. Tsuzuki, H. Tokuda, K. Hayamizu and M. Watanabe, *J. Phys. Chem. B*, 2005, **109**, 16474-16481.
49. S. A. Katsyuba, E. E. Zvereva, A. Vidiš and P. J. Dyson, *J. Phys. Chem. A*, 2006, **111**, 352-370.
50. N. E. Heimer, R. E. Del Sesto, Z. Meng, J. S. Wilkes and W. R. Carper, *J. Mol. Liq.*, 2006, **124**, 84-95.
51. K. Dong, S. Zhang, D. Wang and X. Yao, *J. Phys. Chem. A*, 2006, **110**, 9775-9782.
52. J. Palomar, V. R. Ferro, M. A. Gilarranz and J. J. Rodriguez, *J. Phys. Chem. B*, 2007, **111**, 168-180.
53. P. A. Hunt, I. R. Gould and B. Kirchner, *Aust. J. Chem.*, 2007, **60**, 9-14.
54. L. Zhang, Y. Wang, Z. Xu and H. Li, *J. Phys. Chem. B*, 2009, **113**, 5978-5984.
55. Y. Danten, M. I. Cabaço and M. Besnard, *J. Phys. Chem. A*, 2009, **113**, 2873-2889.
56. Y. Gao, L. Zhang, Y. Wang and H. Li, *J. Phys. Chem. B*, 2010, **114**, 2828-2833.
57. X. Hu, Q. Lin, J. Gao, Y. Wu and Z. Zhang, *Chem. Phys. Lett.*, 2011, **516**, 35-39.
58. K. Dong, Y. Song, X. Liu, W. Cheng, X. Yao and S. Zhang, *J. Phys. Chem. B*, 2012, **116**, 1007-1017.
59. Y.-Z. Zheng, N.-N. Wang, J.-J. Luo, Y. Zhou and Z.-W. Yu, *Phys. Chem. Chem. Phys.*, 2013, **15**, 18055-18064.
60. S. Cha, M. Ao, W. Sung, B. Moon, B. Ahlstrom, P. Johansson, Y. Ouchi and D. Kim, *Phys. Chem. Chem. Phys.*, 2014, **16**, 9591-9601.
61. T. Cremer, C. Kolbeck, K. R. J. Lovelock, N. Paape, R. Wölfel, P. S. Schulz, P. Wasserscheid, H. Weber, J. Thar, B. Kirchner, F. Maier and H.-P. Steinrück, *Chem. – Eur. J.*, 2010, **16**, 9018-9033.

62. C. Hardacre, J. D. Holbrey, M. Nieuwenhuyzen and T. G. A. Youngs, *Acc. Chem. Res.*, 2007, **40**, 1146-1155.
63. C. Hardacre, J. D. Holbrey, C. L. Mullan, T. G. A. Youngs and D. T. Bowron, *J. Chem. Phys.*, 2010, **133**, 074510.
64. T. Köddermann, C. Wertz, A. Heintz and R. Ludwig, *ChemPhysChem*, 2006, **7**, 1944-1949.
65. M. R. Housaindokht, H. E. Hosseini, M. S. Sadeghi Googheri, H. Monhemi, R. I. Najafabadi, N. Ashraf and M. Gholizadeh, *J. Mol. Liq.*, 2013, **177**, 94-101.
66. N. R. Dhumal, K. Noack, J. Kiefer and H. J. Kim, *J. Phys. Chem. A*, 2014, **118**, 2547-2557.
67. E. I. Obi, C. M. Leavitt, P. L. Raston, C. P. Moradi, S. D. Flynn, G. L. Vaghjiani, J. A. Boatz, S. D. Chambreau and G. E. Douberly, *J. Phys. Chem. A*, 2013, **117**, 9047-9056.
68. R. Cooper, A. M. Zolot, J. A. Boatz, D. P. Sporleder and J. A. Stearns, *J. Phys. Chem. A*, 2013, **117**, 12419-12428.
69. K. Fujii, T. Fujimori, T. Takamuku, R. Kanzaki, Y. Umebayashi and S.-i. Ishiguro, *J. Phys. Chem. B*, 2006, **110**, 8179-8183.
70. A. Martinelli, A. Matic, P. Johansson, P. Jacobsson, L. Börjesson, A. Fernicola, S. Panero, B. Scrosati and H. Ohno, *J. Raman. Spectrosc.*, 2011, **42**, 522-528.
71. M. Deetlefs, C. Hardacre, M. Nieuwenhuyzen, A. A. H. Padua, O. Sheppard and A. K. Soper, *J. Phys. Chem. B*, 2006, **110**, 12055-12061.
72. N. Akai, A. Kawai and K. Shibuya, *J. Phys. Chem. A*, 2010, **114**, 12662-12666.
73. Y. Danten, M. I. Cabaço and M. Besnard, *J. Mol. Liq.*, 2010, **153**, 57-66.
74. R. P. Matthews, C. Ashworth, W. Tom and A. H. Patricia, *J. Phys.: Condens. Matter*, 2014, **26**, 284112.
75. P. A. Hunt, B. Kirchner and T. Welton, *Chem. – Eur. J.*, 2006, **12**, 6762-6775.
76. P. A. Hunt and I. R. Gould, *J. Phys. Chem. A*, 2006, **110**, 2269-2282.
77. C. Krekeler, J. Schmidt, Y. Y. Zhao, B. Qiao, R. Berger, C. Holm and L. Delle Site, *J. Chem. Phys.*, 2008, **129**, 174503.
78. S. Zahn, G. Bruns, J. Thar and B. Kirchner, *Phys. Chem. Chem. Phys.*, 2008, **10**, 6921.
79. J. N. A. Canongia Lopes and A. A. H. Pádua, *J. Phys. Chem. B*, 2006, **110**, 7485-7489.
80. V. N. Emel'yanenko, S. P. Verevkin and A. Heintz, *J. Am. Chem. Soc.*, 2007, **129**, 3930-3937.
81. S. Tsuzuki, A. A. Arai and K. Nishikawa, *J. Phys. Chem. B*, 2008, **112**, 7739-7747.
82. R. Ozawa, S. Hayashi, S. Saha, A. Kobayashi and H.-o. Hamaguchi, *Chem. Lett.*, 2003, **32**, 948-949.
83. S. Hayashi, R. Ozawa and H.-o. Hamaguchi, *Chem. Lett.*, 2003, **32**, 498-499.
84. H. Katayanagi, S. Hayashi, H.-o. Hamaguchi and K. Nishikawa, *Chem. Phys. Lett.*, 2004, **392**, 460-464.
85. Y. Umebayashi, H. Hamano, S. Tsuzuki, J. N. Canongia Lopes, A. A. H. Pádua, Y. Kameda, S. Kohara, T. Yamaguchi, K. Fujii and S.-i. Ishiguro, *J. Phys. Chem. B*, 2010, **114**, 11715-11724.
86. N. Hatano, T. Takekiyo, H. Abe and Y. Yoshimura, *Int. J. Spectrosc.*, 2011, **2011**, 648245.
87. I. Skarmoutsos, D. Dellis, R. P. Matthews, T. Welton and P. A. Hunt, *J. Phys. Chem. B*, 2012, **116**, 4921-4933.
88. W. M. Reichert, J. D. Holbrey, R. P. Swatloski, K. E. Gutowski, A. E. Visser, M. Nieuwenhuyzen, K. R. Seddon and R. D. Rogers, *Cryst. Growth Des.*, 2007, **7**, 1106-1114.
89. A. Khrizman, H. Y. Cheng, G. Bottini and G. Moyna, *Chem. Commun.*, 2015, **51**, 3193-3195.
90. X. Zhao, H. Xing, Q. Yang, R. Li, B. Su, Z. Bao, Y. Yang and Q. Ren, *J. Phys. Chem. B*, 2012, **116**, 3944-3953.
91. R. Lü, J. Lin and Z. Qu, *Comput. Theor. Chem.*, 2012, **1002**, 49-58.
92. R. Lü, Z. Qu and J. Lin, *J. Mol. Liq.*, 2013, **180**, 207-214.
93. M. I. Cabaço, M. Besnard, Y. Danten and J. A. P. Coutinho, *J. Phys. Chem. B*, 2011, **115**, 3538-3550.
94. J. Dupont, *J. Braz. Chem. Soc.*, 2004, **15**, 341-350.

95. A. Mele, G. Romanò, M. Giannone, E. Ragg, G. Fronza, G. Raos and V. Marcon, *Angew. Chem., Int. Ed.*, 2006, **45**, 1123-1126.